Journal of Biomedical Optics

BiomedicalOptics.SPIEDigitalLibrary.org

Correcting for motion artifact in handheld laser speckle images

Ben Lertsakdadet
Bruce Y. Yang
Cody E. Dunn
Adrien Ponticorvo
Christian Crouzet
Nicole Bernal
Anthony J. Durkin
Bernard Choi

SPIE.

Ben Lertsakdadet, Bruce Y. Yang, Cody E. Dunn, Adrien Ponticorvo, Christian Crouzet, Nicole Bernal, Anthony J. Durkin, Bernard Choi, "Correcting for motion artifact in handheld laser speckle images," *J. Biomed. Opt.* **23**(3), 036006 (2018), doi: 10.1117/1.JBO.23.3.036006.

Correcting for motion artifact in handheld laser speckle images

Ben Lertsakdadet,[a,b,c] Bruce Y. Yang,[a,c] Cody E. Dunn,[a,b,c] Adrien Ponticorvo,[a,c] Christian Crouzet,[a,b,c] Nicole Bernal,[c,d] Anthony J. Durkin,[a,b,c] and Bernard Choi[a,b,c,*]
[a]Beckman Laser Institute and Medical Clinic, Irvine, California, United States
[b]University of California, Department of Biomedical Engineering, Irvine, California, United States
[c]University of California, Irvine, California, United States
[d]University of California, Department of Surgery, Irvine, California, United States

Abstract. Laser speckle imaging (LSI) is a wide-field optical technique that enables superficial blood flow quantification. LSI is normally performed in a mounted configuration to decrease the likelihood of motion artifact. However, mounted LSI systems are cumbersome and difficult to transport quickly in a clinical setting for which portability is essential in providing bedside patient care. To address this issue, we created a handheld LSI device using scientific grade components. To account for motion artifact of the LSI device used in a handheld setup, we incorporated a fiducial marker (FM) into our imaging protocol and determined the difference between highest and lowest speckle contrast values for the FM within each data set (K_{best} and K_{worst}). The difference between K_{best} and K_{worst} in mounted and handheld setups was 8% and 52%, respectively, thereby reinforcing the need for motion artifact quantification. When using a threshold FM speckle contrast value (K_{FM}) to identify a subset of images with an acceptable level of motion artifact, mounted and handheld LSI measurements of speckle contrast of a flow region (K_{FLOW}) in *in vitro* flow phantom experiments differed by 8%. Without the use of the FM, mounted and handheld K_{FLOW} values differed by 20%. To further validate our handheld LSI device, we compared mounted and handheld data from an *in vivo* porcine burn model of superficial and full thickness burns. The speckle contrast within the burn region (K_{BURN}) of the mounted and handheld LSI data differed by <4% when accounting for motion artifact using the FM, which is less than the speckle contrast difference between superficial and full thickness burns. Collectively, our results suggest the potential of handheld LSI with an FM as a suitable alternative to mounted LSI, especially in challenging clinical settings with space limitations such as the intensive care unit. [DOI: 10.1117/1.JBO.23.3.036006]

Keywords: laser speckle imaging; wide-field imaging; handheld; fiducial marker; blood flow; image alignment; coregistration.

Paper 170678RR received Oct. 17, 2017; accepted for publication Feb. 21, 2018; published online Mar. 15, 2018.

1 Introduction

Laser speckle imaging (LSI) is a wide-field optical technique that enables superficial blood flow quantification. Preclinical applications of LSI include blood flow monitoring in rodent skin[1–4] and in porcine burn models.[5] Potential clinical applications include blood flow monitoring in patients undergoing treatment of port-wine stains[6] and breast tissue perfusion during radiation therapy.[7] A coherent light source (laser) is used to illuminate a tissue region of interest (ROI). LSI devices typically use a two-dimensional sensor array (camera) to capture the interference pattern detected at the imaging sensor plane. The resulting fluctuations in the pattern can be quantified to provide maps of relative blood flow.

Blood-flow information can be helpful in a clinical setting for bedside care. However, since the speckle pattern is sensitive to motion, LSI systems are conventionally designed as mounted, or immobile, often mounted on a tripod or a cart with articulating arm (PeriCam PSI System, Perimed AB, Järfälla, Sweden). Hence, widespread use of LSI in the clinic has not occurred due to the bulky form factor and lack of mobility of the system.

Our proposed solution to address the limitations of these mounted systems is a handheld LSI device. Handheld LSI would provide clinicians with objective blood flow measurements in a convenient form factor. However, using an LSI device in a handheld setup introduces problems due to motion artifact from the user end, which leads to unreliable and inaccurate data observed as variable speckle contrast (K) values. Attempts have been made to account for motion artifact noise. Farraro et al.[8] found that if a particular number of images are acquired per data set, the coefficient of variation in speckle contrast can be reduced to below 5%. Omarjee et al.[9] used adhesive opaque surfaces (AOS) for signal identification during postprocessing of collected LSI data. The AOS was used to denoise LSI data collected to measure cutaneous blood flow.

Although these methods attempt to account for motion artifact, they both lack incorporation of an approach to align (coregister) images. Coregistration is a necessary step prior to the common practice of image averaging to improve the signal-to-noise ratio in LSI flow maps. Our approach to address both motion artifact and image realignment for handheld LSI is the incorporation of a fiducial marker (FM) into our imaging protocol. We hypothesize that, by using an FM, we are able to collect LSI data using a handheld device that approximates the performance of a mounted/fixed LSI system.

*Address all correspondence to: Bernard Choi, E-mail: choib@uci.edu

1083-3668/2018/$25.00 © 2018 SPIE

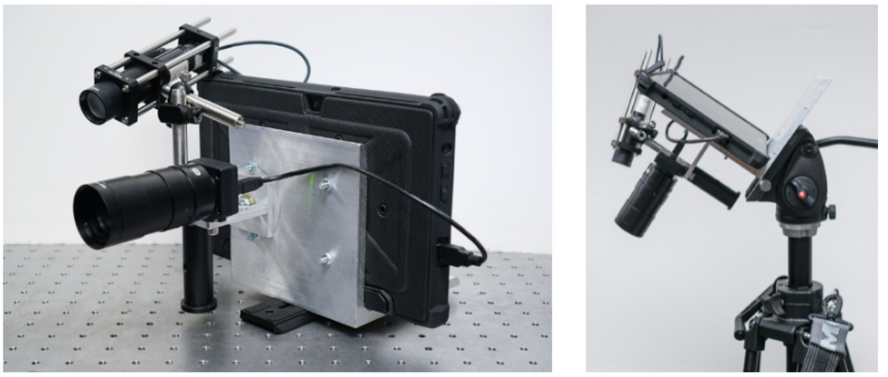

(a) (b)

Fig. 1 Assembled handheld LSI device. (a) Fully assembled device and (b) device in a tripod-mounted setup.

The FM should fulfill the following criteria: (1) it must have a reproducible measured speckle contrast value that can be accurately characterized in a mounted setup; (2) as in Omarjee et al.,[9] the FM must have sufficient thickness and optical scattering to ensure that the K of the FM (K_{FM}) is independent of the underlying tissue; and (3) it must have sufficiently different optical properties from the surrounding tissue regions to facilitate unambiguous identification of the FM during image realignment.

Here we demonstrate that, with integration of an FM into the imaging protocol executed with a handheld LSI device, we can improve the accuracy of K values toward those measured with a gold-standard mounted setup. We compare the performance of the mounted and handheld setups using *in vitro* flow phantom experiments as a proof-of-concept study. We then demonstrated translation of our imaging protocol into an ongoing *in vivo* study with a porcine burn wound model.

2 Materials and Methods

2.1 *Handheld Laser Speckle Imaging Device*

The handheld LSI device (Fig. 1) used in all of the experiments consisted of an 8-bit, 1.32 megapixel CCD camera (CMLN-13S2M-CS, FLIR Integrated Imaging Solutions, Inc., Richmond, BC, Canada) acquiring 640×480 pixel frames at 15 Hz as the imaging sensor. An imaging field of view (FOV) of ~90 mm × 67.5 mm (4:3 ratio) at an imaging distance of 300 mm was obtained using a C-mount lens (Computar C-Mount 13-130 mm Varifocal Lens, Computar). Imaging parameters were selected to achieve ~3 pixels per speckle, thus satisfying the Nyquist sampling criterion.[10] The data were collected and processed on a tablet computer (Microsoft Surface Pro 2, Microsoft Inc.) using a custom-written graphical user interface (GUI) in MATLAB® (The Mathworks, Natick, Massachusetts).

The coherent light source was an 809 nm near-infrared laser diode (140 mW, Ondax Inc., Monrovia, California) positioned at a slightly oblique angle to assist with alignment. A 300-mm ruler was used to check the distance from the LSI device and the sample being measured. If the device was too close during data acquisition, the irradiated region would shift toward the upper left quadrant in the FOV; if the device was too far, the irradiated region would shift toward the lower left quadrant. Data acquisition was initiated only after the irradiation region was in the approximate center of the FOV. The exposure time used for each image was 5 ms, based on the findings of Farraro et al.[8]

The tablet was placed inside a protective case (Urban Armor Gear), which was modified to allow direct mounting of the lens, camera, and laser to the tablet. The device was designed for use in both mounted and handheld configurations.

2.2 *Fiducial Marker*

The FM was an 18% reflectance grey card (Neewer, model #10079934) commonly used in photography. The FM was used to sort and align the acquired images (see Sec. 2.3). It was attached to the surface of a solid silicone phantom (see Sec. 2.4) and imaged using our LSI device in mounted and handheld setups [Fig. 2(a)]. Each data set contained 150 images for analysis. All images were converted into spatial speckle contrast (K) images using a 7×7 pixel sliding window with the equation $K = \sigma/\langle I \rangle$, where K is the contrast, σ is the standard deviation within the window, and $\langle I \rangle$ is the mean intensity of the pixels contained within the window.[1,2,4,6] K_{FM} was quantified from each image.

2.3 *Estimation of Motion Artifact and Image Alignment Using FM*

Motion artifact was estimated using the quantified K_{FM} in each image. All images within a data set were sorted in descending order based on the K_{FM} associated with each image. This approach was based on the assumption that with increasing motion artifact, K_{FM} would decrease from the "true" value (0.50, in this study) measured with the mounted LSI setup. We set arbitrary threshold K_{FM} differences of 10% and 20% (i.e., $K_{FM,thres} = 0.45$ and 0.40, respectively) and determined the number of images in the collected data sets whose K_{FM} values exceeded the threshold, as well as the corresponding K values of a specified ROI extracted from the subset of images (see Secs. 2.4 and 2.5). As a comparison, average K images were also created using all 150 images to compare differences in average K_{FM} values using the FM-based approach and an unsupervised approach.

Prior to ROI extraction from a given subset of LSI images, we used the FM to align the LSI images using custom-written MATLAB® software. First, a median sliding filter with a 7×7 pixel window filter was run on each of the images.

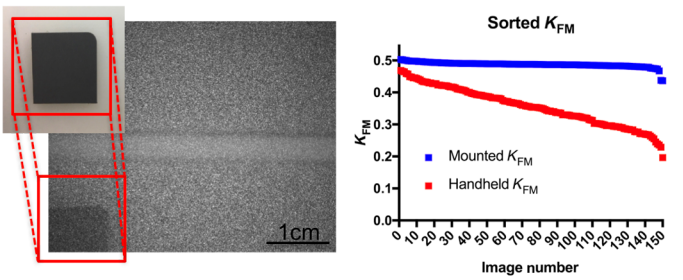

(a) (b)

K_{FM} threshold	% Difference from mounted K_{FM}	# of images
0.40	20	38
0.42	16	24
0.44	12	10
0.46	8	3
0.48	4	0
0.50	0	0

(c)

Fig. 2 FM included into imaging protocol allows for motion artifact detection based on speckle contrast (K). (a) The 18% gray card used in our imaging protocol was placed in the lower left corner of all frames during data acquisition to allow for sorting based on motion artifact and image alignment when calculating average speckle contrast images. Here, the FM was placed on the surface of a flow phantom. The FM was identified and the speckle contrast value of the FM (K_{FM}) was quantified and plotted in descending order for all images within each data set. (b) The handheld K_{FM} values plotted show a rapid decline within a representative sorted handheld data set. The K_{FM} mounted values plotted remain relatively stable across all images within a sorted mounted data set. (c) The table shows candidate values of $K_{FM,thres}$, the percent difference between each of these values and the known K_{FM} value, and the number of images in the handheld data set that exceeds each of the $K_{FM,thres}$ values.

Next, the software calculated the necessary transformation matrices. The transformation matrices were found by performing a translation, rotation, and scaling in multiple axes to align each raw image to the highest ranked raw image.[11] These transformation matrices were created by combining MATLAB® functions with our custom-written software. We converted the raw images to spatial K images and then used the transformation matrices on their respective K images.

2.4 *In Vitro Flow Phantom*

Flow phantom experiments were performed using a solid silicone phantom created with the methods outlined in Ayers et al.[12] We also incorporated a clear plastic tube (diameter 10 mm) as a surface-level inclusion flow tube. The flow medium was a 1% Intralipid solution (Fresenius Kabi) infused into the flow tube using a mechanical pump (NE-1000 Single Syringe Pump, Pump Systems Inc.). Two ranges of flow speeds were used: (1) 0.0 to 1.0 mm/s, in 0.2 mm/s increments and (2) 1 to 5 mm/s in 1 mm/s increments. Sequences of 150 images were acquired using mounted and handheld setups at each flow speed. As described in the previous section, K_{FM} was identified based on specified threshold values and aligned using the FM, followed by quantification of K within an ROI selected inside the flow tube (K_{FLOW}). The difference in K_{FLOW} resulting from data collected with mounted and handheld setups was determined. Bland–Altman analysis[13] was performed with Prism 7 software (GraphPad Software, Inc.) to study the measurement performance of the handheld and mounted LSI setups.

2.5 *In Vivo Mounted Versus Handheld Imaging of Porcine Burn Wound Model*

All experiments were performed in accordance with the Animal Care Use Committee of University of California, Irvine (IACUC # 2015-3154). We performed a graded burn wound experiment using a porcine model described previously.[5] Briefly, 30-mm-diameter burns were created using a brass tool heated to 100°C. The burn severity was based on the contact time of the burn tool to the porcine skin. Contact time was varied from 5 s (superficial) to 40 s (full thickness) to generate a full range of burn severities (16 burns per pig, two pigs). For *in vivo* validation of the handheld LSI approach, we collected data from both superficial and full thickness burns. Each data set was acquired with mounted and handheld LSI setups and contained 100 images to reduce acquisition time. The FM was placed in the FOV of the images and K_{FM} calculated from each image. An average K image was created using the sort, threshold, and align methods described above. Quantification of K from an ROI within each burn (K_{BURN}) was performed and compared for mounted and handheld setups.

3 Results

3.1 K_{FM} *is Indicative of Motion Artifact*

To investigate the influence of motion artifact on handheld LSI measurements, the FM was included in all images acquired for each data set [Fig. 2(a)]. The K_{FM} on a static phantom was quantified with mounted and handheld setups. The true K_{FM} measured with the mounted LSI setup was 0.50. After imaging the marker with these solid phantoms, we sorted the K values of the FM in descending order. K_{FM} decreased more quickly in handheld measurements than in mounted measurements [Fig. 2(b)]. The relative stability of the K_{FM} across the mounted data set [Fig. 2(b)], compared with a handheld data set [Fig. 2(b)], demonstrated the sensitivity of K values to motion artifact. The reduction in K_{FM} in the mounted data set was associated with the button press on the tablet screen to initiate data acquisition. The image with the highest K_{FM} value was considered the "best" image and contained the least motion artifact (K_{best}). The image with the lowest K_{FM} value was considered the "worst" image and contained the most motion artifact (K_{worst}). To analyze the range of motion artifact within each data set, the percent difference between K_{best} and K_{worst} was calculated. In the mounted setup, the percent difference was found to be 8%, whereas the percent difference in the handheld setup was 52%. Furthermore, K_{best} measured with the handheld setup (0.47) was lower than the true K_{FM} value, demonstrating that, even in the best-case comparison, user motion introduces an error.

We then applied threshold K_{FM} ($K_{FM,thres}$) values to identify subsets of images with K_{FM} differences ranging between

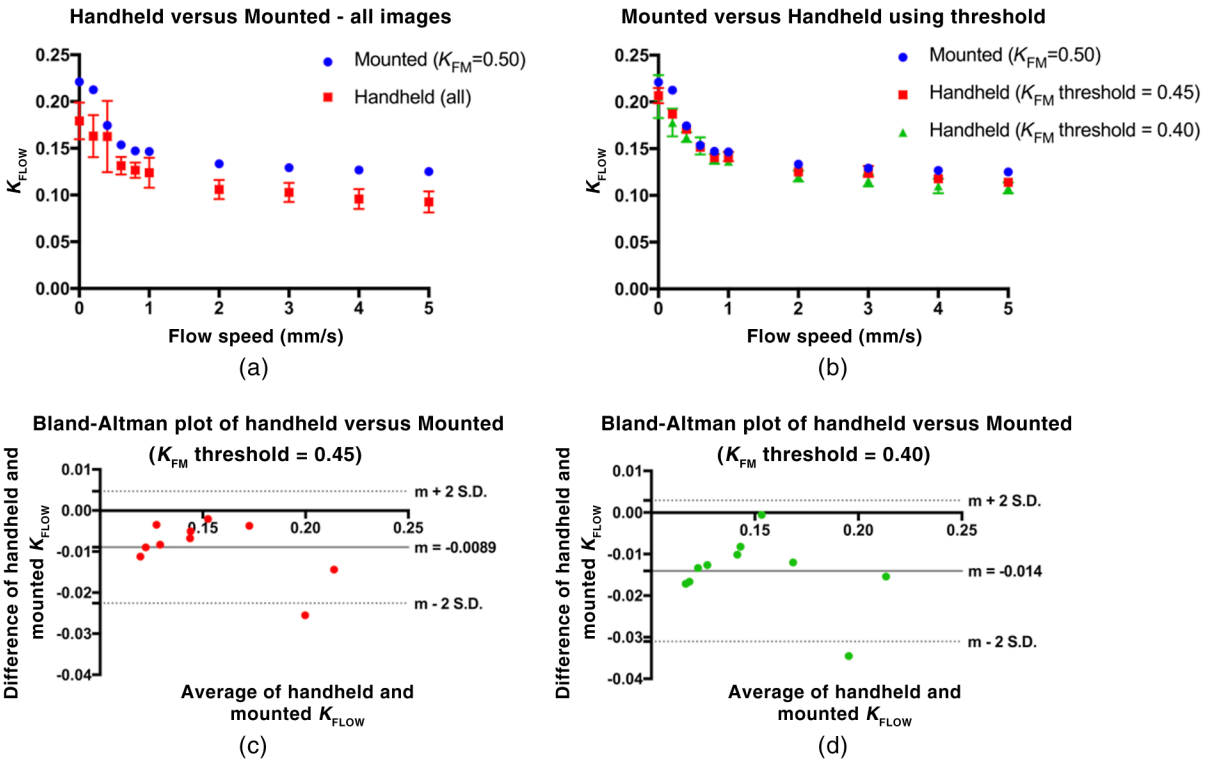

Fig. 3 *K* values of handheld and mounted setups from *in vitro* flow phantom experiments. (a) With an unsupervised approach, use of all 150 handheld LSI images resulted in an error of up to 20%. (b) When using the FM to select a subset of images with a minimum K_{FM} value to account for motion artifact and to realign images, the accuracy of handheld LSI improves, with errors of 8% and 5% for K_{FM} values of 0.40 and 0.45, respectively. (c) Bland–Altman plot of K_{FM} data collected using $K_{FM,thres} = 0.45$. We observed a systematic bias of −0.0089 between the two measurement approaches (95% confidence limits of agreement = −0.023 to 0.0047. (d) Bland–Altman plot of K_{FM} data collected using $K_{FM,thres} = 0.40$. We observed a systematic bias of −0.014 between the two measurement approaches (95% confidence limits of agreement = −0.031 to 0.0029).

0% and 20% [Fig. 2(c)]. As expected, the number of images in each subset decreased as $K_{FM,thres}$ approached the true K_{FM} value. The maximum K_{FM} value from the handheld data sets was consistently below the true K_{FM} value, demonstrating that some motion artifact was present within each image of the handheld data sets. Collectively, these data demonstrate the issues related to motion artifact. If we were to use all of the images within a handheld data set to quantify the mean *K* of an ROI, the handheld setup would potentially result in grossly inaccurate *K* values.

3.2 *Using the FM to Account for Motion Artifact Improves Accuracy of K Values Calculated from Data Acquired with the Handheld LSI Setup*

To investigate how the FM can help with motion artifact correction, the image processing protocol outlined in Sec. 2.3 was applied to use the FM to identify images with the least motion artifact. We first compared the mounted LSI data with $K_{FM} = 0.50$ (i.e., data with no motion artifact) with handheld LSI data using all images, to mimic unsupervised analysis of the data; the median difference in *K* values from an ROI centered on the flow tube inclusion (K_{FLOW}) was 20% (range: 7% to 26%) [Fig. 3(a)]. We then applied $K_{FM,thres}$ values of 0.45 and 0.40 to extract subsets of images with K_{FM} values above these thresholds to analyze further. Each image subset was then aligned using the FM. Using $K_{FM,thres}$ of 0.45 and 0.40 resulted in median differences in K_{FLOW} values of 5% (range: 1% to 12%) and 8% (range: 0.3% to 16%), respectively [Fig. 3(b)], demonstrating the improved accuracy resulting from use of the FM. Bland–Altman analysis with the two thresholds showed biases in K_{FLOW} values of −0.0089 and −0.014 for $K_{FM,thres}$ of 0.45 and 0.40, respectively [Figs. 3(c) and 3(d)]. Since the 95% confidence limits of agreement with both $K_{FM,thres}$ values are similar (−0.023 to 0.0047 for $K_{FM,thres} = 0.45$; −0.031 to 0.0029 for $K_{FM,thres} = 0.40$), we selected $K_{FM,thres} = 0.40$ to apply in the subsequent *in vivo* study described in the next section.

3.3 *Accounting for Motion Artifact with the FM Improved Handheld LSI Performance: In Vivo Porcine Burn Model*

To determine the translational potential of the *in-vitro* findings to *in-vivo* use, we imaged porcine burn wounds. Figures 4(a) and 4(b) show a comparison of speckle contrast maps calculated from speckle image sequences captured with the mounted LSI setup, either without [Fig. 4(a)] or with [Fig. 4(b)] the use of the FM to align the images. Without alignment, the speckle contrast map appears blurred due to movement occurring during data collection. In this specific case, the *K* values were only slightly affected without the use of the FM [median difference in *K* values of 2% (range: 0.1% to 4.0%)], which may have been due to the homogeneity of *K* values within the burned

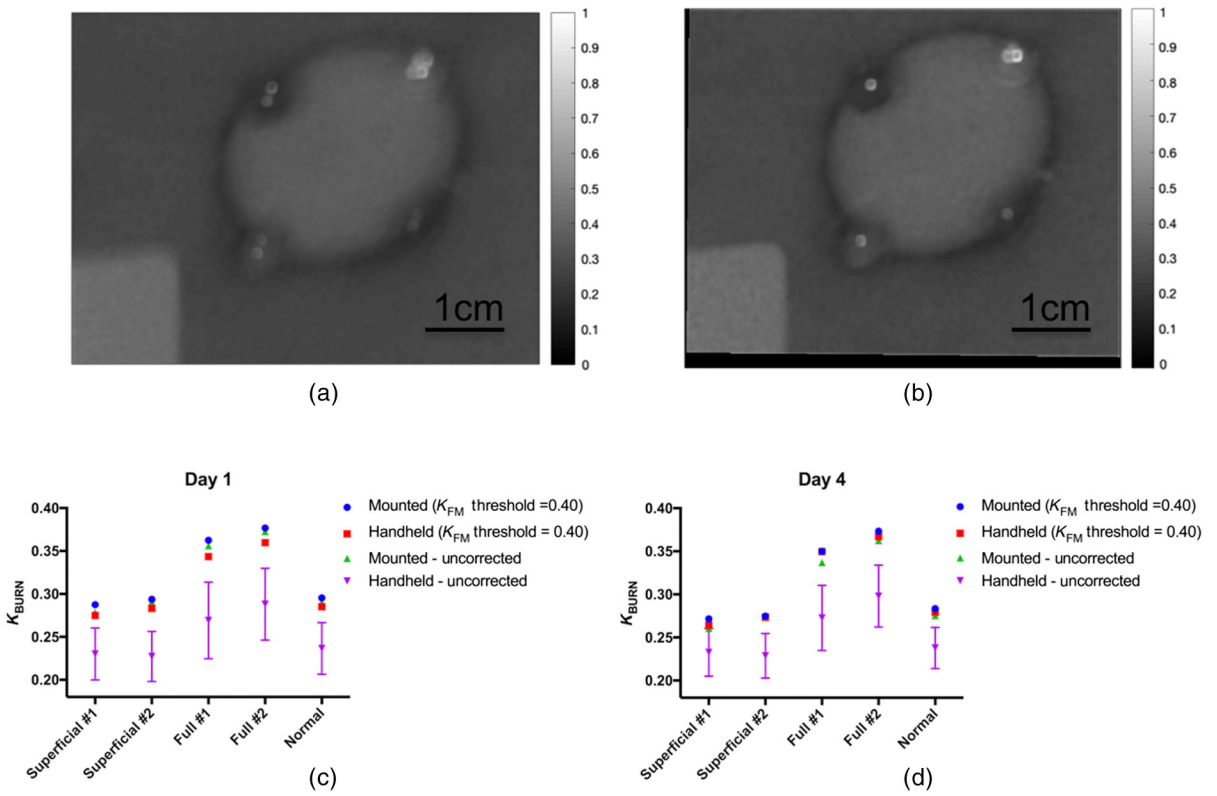

Fig. 4 Mounted versus handheld speckle contrast of superficial and full thickness burns induced on a porcine model. For both the mounted and handheld data sets, we applied $K_{FM,thres} = 0.40$. (a, b) Average K image of sequence of mounted LSI images of a full-thickness burn wound, (a) without and (b) with the use of the FM for alignment and thresholding. Within the image, the larger circular region is the burn region, and the smaller four circular regions are biopsy points taken over the course of the study. (c) Day 1 K_{BURN} data were obtained at ~24 h postburn. The difference in K_{BURN} between thresholded mounted and handheld data sets was 4%, and the difference between superficial and full thickness burns was 27%. (d) Day 4 K_{BURN} data were acquired 4 days postburn, when the burn wounds have stabilized. The difference in K_{BURN} between thresholded mounted and handheld data sets was 1%, and the difference between superficial and full thickness burns was 32%. The uncorrected handheld data reported K_{BURN} values ~20% lower than those reported from handheld data corrected with the use of the FM.

region. In a more heterogeneous flow map, the accuracy is expected to degrade without the use of an alignment technique.

We used our FM and processed the handheld data using $K_{FM,thres}$ of 0.40. This resulted in 10.2 ± 5.4 images used to create the speckle contrast map. Due to motion artifact resulting from subject breathing, K_{best} collected with the mounted setup was 0.46, which is less than the true FM value of 0.50. Hence, we also applied $K_{FM,thres}$ of 0.40 to the mounted LSI data sets.

By imaging superficial and full thickness burns using the LSI device in mounted and handheld setups, we determined the magnitude of K values measured within the burn (K_{BURN}) for both imaging setups. On day 1 postburn, the percent difference of K_{BURN} between the mounted and handheld data was 4% for each burn type. In contrast, K_{BURN} of full-thickness burns was 27% higher than that of superficial burns [Fig. 4(c)].

On the final day (day 4) of imaging, the burn wounds have stabilized and are more indicative of the burn type.[5] The percent difference of K_{BURN} on day 4 for mounted versus handheld was ~1%. K_{BURN} of full-thickness burns was 32% higher than that of superficial burns. These data suggest that, regardless of mounted or handheld LSI setup, we still were able to use K values alone to differentiate between a superficial and full thickness burn. Without the use of the FM to threshold and align the LSI images, handheld LSI reported K_{BURN} values that were ~20% lower (range: 16% to 25%) than handheld LSI with the use of the FM.

4 Discussion

LSI is a simple, noncontact method for mapping superficial blood flow. We previously used LSI in both preclinical and clinical imaging studies, including monitoring of blood flow in a rodent dorsal window chamber model,[1–3] preclinical imaging of a graded burn wound porcine model, and clinical imaging of pulsed-dye laser treatment on port-wine stain patients.[5,6] Although the system components used in these studies and the associated fields of view varied considerably, each system used mounted setups with a stable platform for imaging.

In a clinical setting, the ease and ability of transportation of a device is expected to increase clinical acceptance and use. A handheld LSI device would enable measurements in settings in which it is not possible to use a mounted or bulkier system, such as in the crowded intensive care units and in portable military or civilian medical units. Previous work was done using a first-generation tablet-based, handheld LSI device, capable of performing noncontact, wide-field measurements.[8] The imaging protocol did not consider quantification of motion artifact or alignment of images collected within a given data set.

Mitigating the contributions of motion artifact to measurements of K was achieved only through averaging over 100 raw speckle images to obtain an accurate K value.

Here, we have demonstrated that inclusion of an FM into our imaging FOV and subsequent analysis of measurements from the FM addresses two important aspects that otherwise affect handheld LSI measurements. First, the FM selected has a different K value compared with the silicone phantoms *in vitro* and surrounding tissue *in vivo*. We used the K value of the FM to sort images collected in a sequence in descending order of K_{FM}. This approach allowed us to identify images with the least motion artifact. Second, following identification of the images with the least motion artifact, we used the FM to align these select images. With the FM in the image FOV, image coregistration was achieved by aligning based on the edges of the FM in each image. Collectively, use of the FM accounted for motion artifact and enabled image alignment.

Previous reports on clinical speckle contrast image registration and correction exist in the literature. Richards et al.[14] described image alignment of the speckle contrast images using rigid translation. They did not require the use of an FM because their intraoperative images contained distinct microvascular structure that facilitated image rotation and translation. In speckle contrast images of cutaneous blood flow, distinct architectural landmarks are not always present, so a more generic approach such as the use of an FM is required. Mahe et al.[15] described the use of an opaque material known as Leukotape and the correction of speckle flow values using a simple linear relationship. However, with their method, an individual calibration was required for each subject, which limits the utility of this approach as a general motion artifact removal technique. Omarjee et al.[9] subsequently studied other materials and identified a bilayer material that they could apply toward calibration-free removal of motion artifact from LSI data. Although their approach appears to decrease the noise associated with motion artifact in LSI measurements, they do not present analysis on how different degrees of motion artifact affect K values. In this work, we chose to use the FM strictly to identify the degree to which raw speckle images are affected by motion artifact, to study how the FM can be used to identify a subset of images with an acceptable degree of motion artifact, and to serve as a guide for automated image alignment and quantification from that subset of images.

Methods for blood flow assessment of burn wounds are able to identify a difference in burn severity.[5] Burn severity is normally assessed by the physician, but assessment is accurate only 60% to 80% of the time and only once the burn wound has stabilized days after the initial burn.[16–18] The importance of an acute, objective method for distinguishing different burn severities is that the treatment plan will differ depending on the type of burn. Commercial LSI systems are readily available for burn wound measurements, but these systems are expensive and not easily transportable. We showed that our approach of a handheld LSI device with an FM potentially can enable accurate measurements of K with reduced cost and increased portability. Future studies are warranted.

Other possible applications for handheld LSI in a clinical setting include blood flow imaging of the extremities for patients with diabetes[19] or monitoring of peripheral vascular disease.[20] A need also exists for noninvasive blood flow measurements of preterm neonates with potentially abnormal blood flow due to developmental issues.[21] LSI has the potential to provide important diagnostic information for these and other applications. An advantage of LSI is that it is a noncontact, wide-field imaging methodology, unlike currently used point measurement techniques such as laser Doppler flowmetry. The wide-field nature of LSI inherently provides spatial information potentially at video rates. With integration of a GUI and tablet-based form factor, our intention was to develop an LSI device that could be used by a nonspecialist, such as a member of clinical staff, to facilitate data collection at any time by minimizing barriers to access and use of the device.

Our study has limitations. The current processing time required to sort through each data set and align the images to identify K_{FM} is ~30 s; hence, it is not a real-time protocol. The severity of this limitation can be mitigated with more efficient software development, perhaps using algorithms written in C. Similarly, real-time image alignment would require that revisions be made to the software.

In summary, our *in vitro* and *in vivo* data collectively suggest that handheld LSI with the use of an FM is feasible and a potentially viable approach for bedside blood-flow monitoring. With incorporation of an FM, we can account for motion artifact and reduce its influence on the data, and we can align images to improve the quantitative accuracy resulting from image averaging.

Disclosures

The authors have no relevant financial interests in this article and no potential conflicts of interest to disclose.

Acknowledgments

This material was based on work supported by the Air Force Office of Scientific Research under award numbers FA9550-17-1-0193, FA9550-14-00340, and FA9550-16-1-0342, which funded development of the handheld LSI technology and phantom testing. Support for the graded burn wound on porcine model experiments was provided by NIH/NIGMS R01GM108634. We also acknowledge support from the Arnold and Mabel Beckman Foundation, the NIH Laser Microbeam and Medical Program Grant P41 EB015890, the NIH funded Institute of Clinical and Translational Science TL1 TR001415 Fellowship to Ben Lertsakdadet, the National Science Foundation Graduate Research Fellowship Program under Grant No. DGE-1321846 to Christian Crouzet, and the Cardiovascular Applied Research and Entrepreneurship Fellowship through the Edwards Lifesciences Center for Advanced Cardiovascular Technology's NIH/NHLBI T32 Training Grant No. 5T32HL116270 to Cody Dunn. The content is solely the responsibility of the authors and does not necessarily represent the official views of the NIGMS, NIBIB, or NIH. Any opinions, finding, and conclusions or recommendations expressed in this material are those of the authors and do not necessarily reflect the views of the United States Air Force. We acknowledge visiting scholars Drs. Yasuyuki Tsunoi and Rajan Arora for their contributions to this study.

References

1. A. J. Moy et al., "Wide-field functional imaging of blood flow and hemoglobin oxygen saturation in the rodent dorsal window chamber," *Microvasc. Res.* **82**(3), 199–209 (2011).
2. W. J. Moy et al., "Preclinical in vivo evaluation of Npe6-mediated photodynamic therapy on normal vasculature," *Lasers Surg. Med.* **44**(2), 158–162 (2012).

3. K. M. Kelly et al., "Talaporfin sodium-mediated photodynamic therapy alone and in combination with pulsed dye laser on cutaneous vasculature," *J. Invest. Dermatol.* **135**(1), 302–304 (2014).
4. S. M. White et al., "Imaging to assess blood flow and oxygenation in implantable engineered tissues," *Tissue Eng. Part C Methods* **18**(9), 697–709 (2012).
5. A. Ponticorvo et al., "Quantitative assessment of graded burn wounds in a porcine model using spatial frequency domain imaging (SFDI) and laser speckle imaging (LSI)," *Biomed. Opt. Express* **5**(10), 3467–3481 (2014).
6. B. Yang et al., "Intraoperative, real-time monitoring of blood flow dynamics associated with laser surgery of port wine stain birthmarks," *Lasers Surg. Med.* **47**(6), 469–475 (2015).
7. E. Tesselaar et al., "Changes in skin microcirculation during radiation therapy for breast cancer," *Acta Oncol.* **56**(8), 1072–1080 (2017).
8. R. Farraro, O. Fathi, and B. Choi, "Handheld, point-of-care laser speckle imaging," *J. Biomed. Opt.* **21**(9), 094001 (2016).
9. L. Omarjee et al., "Optimisation of movement detection and artifact removal during laser speckle contrast imaging," *Microvasc. Res.* **97**, 75–80 (2015).
10. S. J. Kirkpatrick, D. D. Duncan, and E. M. Wells-Gray, "Detrimental effects of speckle-pixel size matching in laser speckle contrast imaging," *Opt. Lett.* **33**, 2886–2888 (2008).
11. "Intensity-based image registration—MATLAB imregister," https://www.mathworks.com/help/images/ref/imregister.html (18 September 2017).
12. F. Ayers et al., "Fabrication and characterization of silicone-based tissue phantoms with tunable optical properties in the visible and near infrared domain," *Proc. SPIE* **6870**, 687007 (2008).
13. D. G. Altman and J. M. Bland, "Measurement in medicine: the analysis of method comparison studies," *Statistician* **32**, 307–317 (1983).
14. L. M. Richards et al., "Intraoperative laser speckle contrast imaging with retrospective motion correction for quantitative assessment of cerebral blood flow," *Neurophotonics* **1**(1), 015006 (2014).
15. G. Mahé et al., "Laser speckle contrast imaging accurately measures blood flow over moving skin surfaces," *Microvasc. Res.* **81**(2), 183–188 (2011).
16. A. M. I. Watts et al., "Burn depth and its histological measurement," *Burns* **27**, 154–160 (2001).
17. D. J. Mcgill et al., "Assessment of burn depth: a prospective, blinded comparison of laser Doppler imaging and videomicroscopy," *Burns* **33**, 833–842 (2007).
18. L. Devgan, S. Bhat, and S. Aylward, "Modalities for the assessment of burn wound depth," *J. Burns Wounds* **5**, e2 (2006).
19. A. S. de M. Matheus et al., "Assessment of microvascular endothelial function in type 1 diabetes using laser speckle contrast imaging," *J. Diabetes Complications* **31**(4), 753–757 (2017).
20. S. Katsui et al., "Novel assessment tool based on laser speckle contrast imaging to diagnose severe ischemia in the lower limb for patients with peripheral arterial disease," *Lasers Surg. Med.* **49**(7), 645–651 (2017).
21. M. J. Stark, V. L. Clifton, and I. M. R. Wright, "Microvascular flow, clinical illness severity and cardiovascular function in the preterm infant," *Arch. Dis. Child. Fetal Neonatal Ed.* **93**, F271–F274 (2008).

Biographies for the authors are not available.